Temporal expectations modulate coupling between frontal and sensory brain areas

Péter Nagy[a,b,†,*], Petra Kovács[a,c,e,f,†], Ádám Boncz[a], Orsolya Szalárdy[a,d], Robert Baumgartner[e], Karolina Ignatiadis[e], István Winkler[a], Brigitta Tóth[a]

[a]Institute of Cognitive Neuroscience and Psychology, HUN-REN Research Centre for Natural Sciences, Magyar tudósok körútja 2., H-1117 Budapest, Hungary

[b]Department of Artificial Intelligence and Systems Engineering, Faculty of Electrical Engineering and Informatics, Budapest University of Technology and Economics, 1117 Budapest, Magyar tudósok körútja 2., Hungary

[c]Department Of Cognitive Science, Faculty of Natural Sciences, Budapest University of Technology and Economics, Műegyetem rkp. 3., H-1111 Budapest, Hungary

[d]Institute of Behavioural Sciences, Faculty of Medicine, Semmelweis University, H-1089 Budapest, Nagyvárad tér 4., Hungary

[e]Acoustics Research Institute, Austrian Academy of Sciences, Dominikanerbastei 16, 1010 Vienna, Austria

[f]Department of Behavioral and Cognitive Biology, Faculty of Life Sciences, University of Vienna, Universitätsring 1, 1010 Vienna, Austria

[†] Peter Nagy and Petra Kovacs should be considered joint first authors.

***Corresponding author:** Péter Nagy, Institute of Cognitive Neuroscience and Psychology, HUN-REN Research Centre for Natural Sciences, Magyar tudósok körútja 2., Budapest H-1117, Hungary. Telephone: +36 1 382 6808, Fax: +36 1 3826295, ORCID: 0000-0003-1902-0469, Email: nagy.peter.ssprg@ttk.hu

Abstract

Temporal prediction is a crucial mechanism that allows the brain to optimize sensory processing by anticipating event timing. This predictive ability enhances processing efficiency by modulating brain activity through cortical oscillations that periodically influence neuronal excitability . For example, stimuli with predictable timing are processed more accurately. Although it is well-established that predictions are generated across large-scale brain networks, the roles of different cortical regions, particularly the frontal cortices and sensory areas, remain debated. In this study, we investigated the role of frontal cortices in temporal prediction during auditory perception. Cue tones predicted the timing of auditory targets with different levels of certainty (50%, 80%). We recorded electroencephalographic data (EEG) while participants detected the targets. Functional connectivity analyses revealed that the level of predictability modulates the relative contributions of frontal and auditory cortices during both the anticipation and detection of targets: as the certainty of predictions grows, the involvement of frontal brain regions increases. Our findings suggest that the auditory temporal prediction network relies on an integrated system of frontal and sensory regions, which are sensitive to the level of predictability.

Keywords: temporal prediction, NDTE, frontal cortex, cued target detection, auditory perception, EEG, transfer entropy

1. Introduction

During perception, predicting when an event will occur enables the nervous system to optimize the processing of this event (Jones, 2018; Large & Jones, 1999). Temporal prediction can increase processing efficiency by manipulating the cortical oscillatory mechanisms that cause neuronal populations to periodically enter states of higher and lower excitability (Buzsáki & Draughn, 2004; Schroeder & Lakatos, 2009). For instance, simple visual stimuli are identified more accurately if their timing is predictable (Toosi et al., 2017). Predictions about the environment are generated and propagated through large-scale functional brain networks, involving an intricate interplay between various higher-order and sensory brain regions. However, these large-scale networks are still poorly understood. In the present study, we aim to test the role of functional connectivity of frontal cortices that correlates with temporal prediction processes.

Different studies of perceptual prediction emphasize distinct roles for the frontal cortex and sensory areas. Some studies suggest that the frontal cortex is crucial for predictive processes: for instance, temporal predictions are subserved by prefrontal areas in monkeys (Meirhaeghe et al., 2021), while in humans, the inferior frontal – as well as the inferior parietal – cortex has been shown to have a similar function (Coull et al., 2016). Conversely, other studies emphasize the role of sensory areas in predictive processes. There is evidence that predictive processing can occur separately within the visual and auditory cortices, supporting the argument that sensory areas can generate predictions and error signals independently of higher-order cortical involvement (De Lange et al., 2018; Kok et al., 2012; Murray and Keller, 2011; Rao and Ballard, 1999). Finally, integrative approaches propose that both the frontal cortex and sensory areas play complementary roles in perceptual prediction (Clark, 2013; Hohwy, 2013). In both the visual and auditory domains, increased connectivity was found between frontal and sensory cortices when subjects had some prior expectation for the upcoming stimulus (Osnes et al., 2012; Rahnev et al., 2011).

Regardless of which cortical areas participate in the fine-tuning of perception based on temporal predictions, information within and between these areas is thought to be propagated through neural oscillations (Buzsáki & Draughn, 2004). The mechanistic role of these oscillations in temporal prediction has been characterized at a local level in studies using electroencephalography (EEG). Arnal and Giraud (2012) highlight that the phase of slow oscillations (delta-theta, 2–8 Hz) in the auditory cortex resets before an expected auditory stimulus but not before an unexpected one, and stimuli presented in the highest-excitability phases of delta oscillations yield faster reaction times than

those presented in a low-excitability phase (see also Lakatos et al., 2005). Stefanics and colleagues (2010) found that the phase of delta oscillations reflects the predictability of events: More predictable timing corresponds to greater phase synchronization between rhythmic auditory events and delta oscillations in the auditory cortex.

While phase resetting and synchronization at a local level are well-established, a related but distinct process also mediated by oscillations is functional connectivity—the interaction among different brain areas. Functional connectivity refers to the synchronization of activity between spatially distinct regions, even when not directly linked to an external stimulus (Sauseng & Klimesch, 2008). Brain regions involved in these synchronization processes most dominantly are termed hubs. This form of connectivity is critical for understanding the functional roles of cortical areas in broader networks, especially for tasks requiring temporal coordination across regions. Functional connectivity mediated not only by slow delta oscillations but also higher-frequency alpha and gamma oscillations has been shown to play a crucial role in predictive processing. For instance, alpha band power has been associated with mechanisms for updating auditory timing (Arnal et al., 2015), while gamma band power has been linked to subsecond auditory perceptual timing (Kaiser et al., 2007). However, whether and how predictability is encoded within these large-scale functional networks remains unclear. Here, we aim to address this question by extending the methods of Stefanics and colleagues (2010) to explore functional connectivity patterns between auditory and frontal regions.

Rich-club brain networks are functional networks whose hubs are more densely connected with each other than with regions outside of the network (van den Heuvel & Sporns, 2011). As such, these networks play a crucial role in information integration across different brain areas, which is essential for complex cognitive functions. Rich-club hubs are important for perceptual predictions and decision-making involving a cascade of events in a distributed neural network (Philiastides & Sajda, 2007). Therefore, they might play a role in integrating sensory input with prior knowledge, especially in temporal predictions where timing and sequencing of sensory information are critical. While functional magnetic resonance imaging (fMRI) provides detailed spatial information about these networks, electroencephalography (EEG) captures fast temporal dynamics, offering complementary insights (Mantini et al., 2010).

These studies and theories reflect the ongoing debate about the roles of different brain regions in perceptual prediction, highlighting the contributions of both the frontal cortex and sensory areas. Here, we aim to identify the functional hubs that contribute to the temporal prediction network by utilizing the high temporal resolution of EEG and data-driven approaches for connectivity analyses (Deco et al., 2021; Deco et al., 2022; Ignatiadis et al., 2024). The present study investigated the role of frontal cortices in temporal prediction during auditory perception. To this end, participants completed a cued auditory target detection task while high-density EEG was recorded. A cue sound predicted the likelihood of a target sound appearing after a shorter or longer interval. Targets were classified into three conditions based on the predictability of the target's timing: 100%, 80%, or 50% predictability. By differentiating between predictable and less predictable events in this task design, we aimed to explore the frontal and sensory network hubs involved in processing and updating temporal predictions and whether the temporal prediction network is affected by the level of predictability.

2. Methods

2.1. Participants

Twenty healthy young adults participated in the study, recruited from a pool of participants who participated in our previous experiments (10 female; mean age: 22.4 ± 2.35 years, all right-handed). Participants were financially compensated for their participation (approx. 4 euros per hour). None of the participants reported any neurological diseases or hearing problems. Participants signed written informed consent forms after the tasks and aims of the experiment were explained to them. The study followed the Declaration of Helsinki guidelines and was approved bythe local ethics committee of the Institute of Cognitive Neuroscience and Psychology of the Research Centre for Natural Science (United Ethical Review Committee for Research in Psychology; EPKEB). The EEG data of 3 participants were excluded from the analysis due to technical issues (missing blocks) during data acquisition. The final group for which EEG was analyzed was thus composed of 10 female and 7 male listeners, mean age 22.6 ± 2.45 years.

2.2. Stimuli and procedure

Participants performed an auditory target detection task while EEG was recorded. Figure 1A shows the experimental design. Participants were instructed to detect the target as soon as possible by pressing a key on a computer keyboard with the pointer finger of the dominant hand. The target was always preceded by a cue. The interval between the cue and the target (inter-stimulus interval, ISI) was either 1200 or 2400 ms (early vs. late target). The intertrial interval was randomized between 200-1000 ms. All stimuli were presented at a uniform listening level (~70 dB).

Two types of cues were used to predict the probability of the target stimulus appearing either after the short or the long ISI (early vs. late target). The cue was a tone with a frequency of 1048 Hz or 1318 Hz and was presented for 100 ms with 10 ms rise/fall times. The target tone was always 1876 Hz and was also presented for 100 ms with 10 ms rise/fall times. The frequencies of cue tones were chosen to be separated by one semitone, whereas the target tone was two semitones higher than the highest cue tone, making the tones clearly distinguishable. One of the tones was predictive, the other unpredictive of the target's delay from the cue; the order of the two equiprobable cues was randomized separately for each participant (Fig. 1A). Following a predictive cue, the ISI was short on 80% of the trials, that is, early targets were more frequent than late targets. Following an unpredictive cue, early and late targets appeared with equal probability (50%). There were three blocks of 50 trials in each condition. Condition order was randomized across participants. A total of 300 responses to targets (150 per cue type, resulting in min. 75 epochs per condition) were collected from each participant. Before testing and data recording, participants were familiarized with the stimuli and the task by a few trials.

In this design, we can distinguish three kinds of target events according to their within-trial predictability. If the cue was not followed by an early target (short ISI), there was always a late target (long ISI) instead, with known onset. Thus, late targets were 100% predictable by the time they were presented. Early targets were 80% predictable if preceded by a predictive cue, and 50% predictable if preceded by an unpredictive cue. We will refer to these three types of targets as the 100%, 80%, and 50% predictable conditions, respectively (Fig. 1A, right panel). For the 100% predictable condition, we used the trials from the late targets after the unpredictive cue because this gave us the most epochs/trials possible (50% of the 150 trials, as opposed to 20% after the predictive cue).

2.3. EEG recording and preprocessing

For EEG recording, a BrainAmp DC 64-channel EEG system with actiCAP active electrodes was used. The sampling rate was 1 kHz, with a 100 Hz online low-pass filter applied. Electrodes were placed according to the international 10/20 system. The FCz channel served as the reference electrode. Bipolar recording from two electrodes placed lateral to the eyes' outer canthi served to monitor eye movements. During the recording, impedances were kept below 15 kΩ.

EEG data preprocessing was conducted with the EEGLAB 14.1.2. toolbox (Delorme et al., 2007) implemented in MATLAB (2021b, Mathworks, Natick, Massachusetts, USA). Offline band-pass filtering was applied between 0.5 and 80 Hz using a finite impulse response (FIR) filter (Kaiser window, Kaiser $\beta = 5.65$, filter length 4530 samples). The data were then re-referenced to the average of all EEG channels. The Infomax algorithm for independent component analysis (ICA) was employed for artifact removal (Delorme et al., 2007). ICA components constituting blink artifacts were removed after a visual inspection of their topographical distribution and the frequency contents of the components. A maximum of 6 components per subject was removed in this way (<10%). Malfunctioning channels were also identified based on ICA components. A maximum of two malfunctioning EEG channels were allowed per participant without exclusion from the study. These were interpolated using the default spline interpolation algorithm implemented in EEGLAB.

2.4. Data analysis

2.4.1. Behavioral data

Statistical analyses were performed in STATISTICA (version 13.1, TIBCO Software Inc., Palo Alto, California, USA). A 2x2 repeated-measures ANOVA was used to compare the effects of cue type (predictive vs. unpredictive) and target type (early vs. late) on reaction time (RT) measured from target onset. Response times longer than 1000 ms from target onset were discarded from analysis (Fig. 1A). The alpha level was set to 0.05. All significant results are reported. Sphericity violations were tested for all comparisons, and correction on the degrees of freedom was applied as necessary (the ε correction factor is then reported). Partial eta squared (η_p^2) is reported as the measure of effect size. Post-hoc tests were computed by Tukey "Honest Significant Difference" (HSD) pairwise comparisons (Tukey, 1949).

2.4.2. ERP cluster analysis

For event-related potential (ERP) analysis, the EEG data was filtered for the delta band (0.5-4 Hz) following Stefanics and colleagues (2010). From the continuous EEG recordings, epochs were extracted between -500 and +1000 ms relative to the onset of target events based on within-trial predictability (50%, 80%, and 100% predictability conditions). Epochs including an amplitude change of 100 μV or greater were rejected from further analysis. ERP cluster analysis was applied to compare potentials evoked by targets in three comparisons: 50% vs. 80% predictable, 50% vs. 100% predictable, and 80% vs. 100% predictable conditions. Because the number of epochs in the 80% predictable condition was higher than in the other two conditions, the number of epochs was equalized between conditions: in each subject, epochs were randomly removed from the 80% predictable condition so that the same number of epochs remained as in the 50% predictable condition for the same subject. The number of epochs varied from subject to subject but was consistent within subjects in each condition (M = 74.17; SD = 1.12).

The cluster-based analysis was performed in the MATLAB toolbox Brainstorm (Tadel et al., 2011; version 10-Mar-2022). For each comparison, a permutation test was applied to the epochs (0-1000 ms). The conditions were compared with two-tailed paired t-tests using 1000 permutations. The minimum number of neighboring channels was set to 3, and the alpha level was set to 0.05.

2.4.3. EEG source localization and functional connectivity analysis

For functional connectivity analysis, data were band-pass filtered between 0.5 and 45 Hz using an FIR filter (Hamming window, filter length 6600 samples) before segmenting into epochs. The 45 Hz cutoff frequency was chosen to attenuate high-amplitude transient noise peaks in the EEG while keeping frequencies between the delta and gamma bands. Epochs between -500 and +4500 ms were extracted, relative to the onset of cue events (predictive and unpredictive) for each condition. Epochs with a >100 uV amplitude change were discarded from further analysis. After discarding epochs, at least 58 epochs remained for each participant in each condition. For comparability, 58 epochs were randomly selected and kept for each participant in each condition to avoid any sample size bias within or between participants. The Brainstorm toolbox (Tadel et al., 2011; version 10-Mar-2022) was used to perform EEG source reconstruction, following the protocol of previous studies (Song et al., 2015; Huang et al., 2016; Pizzagalli., 2007; Tóth et al., 2020). The forward boundary element head model (BEM) was used as provided by the openMEEG algorithm (Fuchs et al., 1998, 2002; Gramfort et al., 2010). Individual structural MRI and default electrode positions were available for each participant and used for head modeling. Anatomical magnetic resonance images (MRIs) were segmented via Freesurfer (Fischl, 2012). The recorded activity was inferred to the cortical surface via dynamic statistical parametric mapping (dSPM) (Dale et al., 2000). The noise covariance was calculated from a 200 ms interval preceding the onset of cue events. Dipole orientations were considered constrained to the surface and source signals were reconstructed at 15000 vertices describing the pial surface. By averaging dipole strengths across voxels, the mean source waveforms were obtained for 62 cortical areas (regions of interest, ROIs) based on the anatomical segmentation of the Desikan-Killany-

Tourville atlas (DKT atlas, Klein and Tourville, 2012). Mean source waveforms corresponding to the 62 ROIs were used for functional connectivity analysis.

Neural oscillations with various frequencies have been linked to timing mechanisms (Wiener & Kanai, 2016), e.g. the power of alpha band oscillations has been associated with auditory timing update mechanisms (Arnal et al., 2015); the power of gamma band oscillations has been linked to subsecond auditory perceptual timing mechanisms (Kaiser et al., 2007); delta-beta coupled oscillations have been associated with temporal prediction accuracy (Arnal et al., 2015). For functional connectivity, two frequency bands were investigated: the delta band (0.5-4 Hz, 2nd order zero-phase Butterworth filter) to analyze functional connectivity based on the ERP analysis results, and broadband (0.5-45 Hz) to examine higher frequencies. For the delta band, the time window of interest was defined between 100 and 1300 ms after stimulus onset (cue or target). For broadband, the time window of interest was defined between 100 and 1300 ms after cue onset, and it was defined based on the results of the ERP analysis for the post-cue period (between 200 and 500 ms after target onset). The time windows of interest were selected considering the dynamics of anticipatory neural processes, the ERP analysis results, and the EEG signal's frequency content. In the post-cue period, the anticipatory process can be assumed to build up gradually and continuously (Walter et al., 1964; Kononowicz and Penney, 2016). Therefore, the whole post-cue period was used for functional connectivity analysis, both for the delta band and broadband data. In the post-target period, the difference between neural responses to target presentation corresponding to different conditions can be assumed to be more localized in time compared to the post-cue period. Based on the results of the ERP analysis, the time window between 200 and 500 ms after target onset was selected for functional connectivity analysis of broadband data (the frequency content of broadband data enables the investigation of short time windows). Due to the low-frequency oscillations in the delta band, this 300 ms-long time window could not be used; therefore, we selected the same time window as for the post-cue period (between 100 and 1300 ms after target onset).

Functional connectivity was analyzed using the Normalized Directed Transfer Entropy (NDTE) framework (Deco et al., 2021; see Ignatiadis et al. (2024) for an application on EEG data). The NDTE framework provides a bidirectional (inflow/outflow) description of the functional information flow. The NDTE flow F_{XY} from time series X to Y (from a source brain area to another target brain area) is defined as

$$F_{XY} = I(Y_{i+1};X^i|Y^i) / I(Y_{i+1};X^i,Y^i) \qquad (1)$$

where the mutual information $I(Y_{i+1};X^i|Y^i)$ corresponds to the degree of statistical dependence between the past of X and the future of Y, and $I(Y_{i+1};X^i,Y^i)$ corresponds to the joint mutual information that the past of both signals together, X and Y, have about the future of Y. The normalization by $I(Y_{i+1};X^i,Y^i)$ enables one to compare and combine the directed mutual information flow across different pairs of brain regions. With this notation, Y_{i+1} denotes the activity level of brain area Y at time point $i+1$, and X^i denotes the whole activity level of the past of X in a time window of length T up to and including time point i (that is, $X^i = [X_i\ X_{i-1}\ \ldots\ X_{i-(T-1)}]$). Following Deco et al. (2021), we estimated the value of T (order, or maximum lag) based on the decay to the first minimum of the autocorrelation function across conditions and subjects.

$I(Y_{i+1};X^i|Y^i)$ can be calculated based on conditional entropies:

$$I(Y_{i+1};X^i|Y^i) = H(Y_{i+1}|Y^i) - H(Y_{i+1}|X^i,Y^i) \qquad (2)$$

where the conditional entropies are defined as follows:

$$H(Y_{i+1}|Y^i) = H(Y_{i+1},Y^i) - H(Y^i) \qquad (3)$$

$$H(Y_{i+1}|X^i,Y^i) = H(Y_{i+1},X^i,Y^i) - H(X^i,Y^i) \qquad (4)$$

and the conditional entropies can be estimated based on covariance matrices of X and Y (Brovelli et al., 2015). $I(Y_{i+1};X^i,Y^i)$ is the sum of the predictability of Y_{i+1} by the past of $X^i|Y^i$ and the internal predictability of Y_{i+1}, that is $I(Y_{i+1};Y^i)$:

$$I(Y_{i+1};X^i,Y^i) = I(Y_{i+1};Y^i) + I(Y_{i+1};X^i|Y^i) \qquad (5)$$

In our study, NDTE values were standardized using circular-shift surrogate data (Deco et al., 2021; Deco et al., 2022; Ignatiadis et al., 2024). The advantage of time-shifted surrogates is that the properties (e.g. amplitude and autocorrelation spectrum) of each signal are maintained because the signals are exactly the same, but the cross-correlation between the signals is reduced to chance level (Quiroga et al., 2002). In our study, 100 independent circular time-shifted surrogate iterations were performed for each considered ROI pair in each trial, and real NDTE values were standardized by

subtracting the mean and dividing by the standard deviation of the corresponding 100 surrogate NDTE values.

Standardized NDTE values were used to identify functional hub regions in the brain. Following the concept of the functional rich club (FRIC) introduced by (Deco et al., 2021), we aimed to identify the core set of brain regions that are more densely functionally connected among themselves than to other brain regions. As a first step of the FRIC analysis, standardized NDTE values were averaged across trials and subjects resulting in one standardized NDTE matrix of dimensions ROI x ROI for each condition. Following the notations of Deco and colleagues (2021), this matrix is denoted by C_{All}. For each ROI i of C_{All}, the total inflow from all ROIs of the cortical parcellation is defined as the sum of connectivity across all columns of the matrix: $G_{in}(i) = \Sigma_j C_{All(i,j)}$. The total outflow per ROI i is defined as the sum of connectivity across all rows of the matrix: $G_{out}(i) = \Sigma_j C_{All(j,i)}$.

The major hubs were defined through an iterative process. After sorting the regions based on their inflow from higher to lower, an algorithm searched for the largest subset of ROIs k that had a value $G_{FRIC}(k)$ significantly larger than any other set with the same number of regions. $G_{FRIC}(k)$ is defined as follows:

$$G_{FRIC}(k) = \Sigma_k C_{All(k)} + \Sigma_k G_{in}(k) - \Sigma_k G_{out}(k) \qquad (6)$$

where $\Sigma_k C_{All(k)}$ is the sum of connections between all club members, $\Sigma_k G_{in}(k)$ is the sum of all incoming connections of the club members, and $\Sigma_k G_{out}(k)$ is the sum of all outgoing connections of the club members. The significance value of each $G_{FRIC}(k)$ was assessed via 1000 Monte Carlo simulations. In each permutation, surrogate clubs with k members were created that had the same $k-1$ members with one added random new member. Starting with the ROI having the largest incoming NDTE flow, the algorithm ran while the p-value of the comparison between the considered FRIC and surrogate clubs was smaller than 0.05.

Based on the results of the FRIC analysis, the functional information inflow of frontal regions (the union of frontal FRIC regions across conditions: caudal middle frontal gyrus, insula, pars opercularis, pars orbitalis, pars triangularis, rostral middle frontal gyrus) was further investigated. Permutation-based t-test analysis (Maris and Oostenveld, 2007) was applied to compare both the total inflow, and individual inflow edges in three comparisons: 50% vs. 80% predictable, 50% vs. 100% predictable, and 80% vs. 100% predictable conditions. An alpha level of 0.05 was used. Significance values were corrected against multiple comparisons using the Benjamini-Hochberg method (Benjamini and Hochberg, 1995).

3. Results

3.1. Behavioral results

Two different cue tones predicted the timing of the target tone with different probabilities, resulting in targets with 50% vs. 80% within-trial predictability after short ISI (early targets) and targets with 100% within-trial predictability after long ISI (late targets). In the case of early targets, we expected that predictive cues lead to faster responses. A repeated-measures ANOVA with factors CUE TYPE (predictive vs. unpredictive) and TARGET TYPE (early vs. late) was calculated from the RT data. The ANOVA revealed a significant interaction between CUE TYPE and TARGET TYPE ($F(1,19) = 11.20$; $p < 0.01$; $\eta_p^2 = 0.37$), as well as a significant main effect of CUE TYPE ($F(1,19) = 5.92$; $p < 0.05$; $\eta_p^2 = 0.24$). A post-hoc test revealed that the effect was caused by significantly slower RTs for unpredictive cues at the early target condition compared with the predictive cues at the early target condition ($t(19) = 4.97$; $p < 0.001$; Cohen's d = 0.70; Fig. 1B).

Further, we expected that RT would be faster for late targets than for early ones, as late targets are 100% predictable by the time they are presented. Accordingly, RT for late targets (50% within-block probability after the unpredictive cue) was significantly shorter than for early targets (50% within-block probability after the unpredictive cue; $t(19) = 5.05$; $p < 0.001$; Cohen's d = 0.58; Fig. 1B). After a predictive cue, RTs to early and late targets were not significantly different ($p > 0.05$).

3.2. ERP results

The ERP data were analyzed using a cluster-based permutation test in three comparisons based on within-trial probability: 50% vs. 80% predictability, 50% vs. 100% predictability, and 80% vs. 100% predictability. The cluster-based permutation test showed a significant difference for all three comparisons ($p < 0.05$, at least; Fig. 1C). The clusters found in the 50% vs. 80% predictability comparison were spatially and temporally similar to those in the 50% vs. 100% predictability comparison. In both cases, two clusters were found, each ($p < 0.01$, all). The clusters started at around 200 ms after target onset, lasting about 300 ms (Fig. 1C, lower panels). One cluster in each comparison contained mainly frontal electrodes, while the other cluster in each comparison consisted of central and posterior electrodes (Fig. 1C, left and middle panel). Frontal and parietal clusters share the same time range, but at opposite polarities. The 80% and 100% predictability conditions also differed significantly from each other, corresponding to one cluster of right lateral electrodes, extending temporally from about 200-400 ms after target onset ($p < 0.05$; Fig. 1C, right panel).

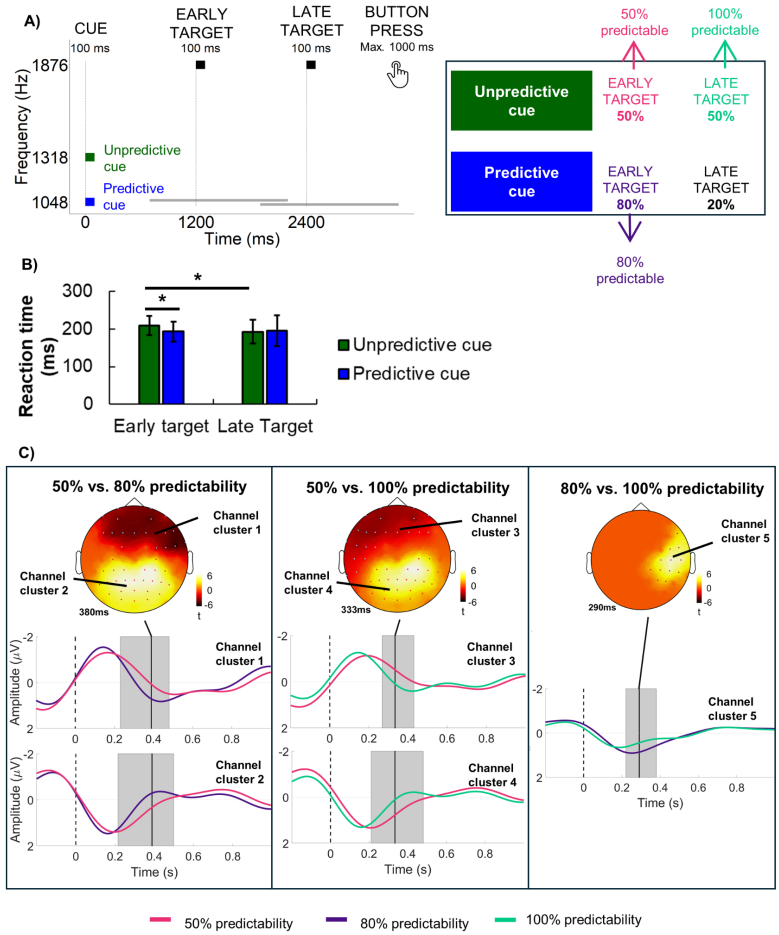

Figure 1. Stimuli, reaction time results and ERP cluster results. **A)** Timeline of the stimulus presentation. In each trial, one cue and one target were presented, each 100 ms in length. The target followed the cue after short or long ISI (early vs. late target). Time windows for the ERP cluster analysis are marked by gray horizontal lines (-500 to 1000 ms relative to the onset of targets). Two types of cues were used: unpredictive and predictive cues. The cues differed in their pitch. After a predictive cue, an early target followed with 80% certainty, and after an unpredictive cue, early and late targets followed with equal likelihood. We refer to the 50%, 80% and 100% predictable conditions according to their within-trial probability as shown in the figure (right panel). **B)** Mean RTs to the target events. **C)** Maps of t-values derived from the cluster-based permutation test, with the ERP channel clusters shown at the time point of the largest spatial extent (top panels). ERP timelines of the corresponding channel averages per cluster are shown in the bottom panels, with time clusters highlighted in grey.

3.3. Functional connectivity results

The order / maximum lag of the models in the NDTE framework was estimated based on the decay to the first minimum of the autocorrelation function. The mean and standard deviation of these

decay times were 57.64 ± 31.94 ms for the post-cue period in the delta band, 54.35 ± 31.47 ms for the post-target period in the delta band, 14.15 ± 1.18 ms for the post-cue period of broadband data, and 15.16 ± 3.06 ms for the post-target period of broadband data. In the NDTE framework, inflow (G_{in}) represents the connectivity incoming into a ROI. We identified the primary inflow hubs for each condition and the average of all conditions using the FRIC procedure. FRIC analysis identified the core set of brain regions (network) that are more densely functionally connected among themselves than to other brain regions. Inflow hubs were identified based on the average of all epochs of all subjects in a given condition. Results are reported for the delta band (Fig. 2, Table A1, Table A2) and for broadband data (Fig. 3, Table A3, Table A4). Regardless of frequency band the 80% and 100% predictability conditions showed stronger frontal involvement than the 50% predictability conditions, especially for broadband data. This observation was further investigated by comparing the frontal regions' total inflow and individual inflow edges in the three conditions.

The analysis of total inflow of the selected set of frontal regions (the union of frontal FRIC regions across conditions: caudal middle frontal gyrus, insula, pars opercularis, pars orbitalis, pars triangularis, and rostral middle frontal gyrus; each region on both hemispheres) revealed significantly higher total inflow in the 80% predictable condition compared to the 50% predictable condition ($p < 0.05$) for broadband data in the post-target 0.2 - 0.5 s period (Fig. 4). None of the other meaningful contrasts yielded a significant result for broadband data ($p > 0.05$, all), and no significant difference was found in any contrast for the delta band ($p > 0.05$, all).

The analysis of individual inflow edges of frontal regions revealed significant differences between conditions only for broadband data in the post-target 0.2 - 0.5 s period. For the 50% vs. 100% predictability difference, no edge showed a significant difference. For the 50% vs. 80% predictability difference, significant edges correspond to the right caudal middle frontal gyrus, right insula, right pars opercularis, and left pars orbitalis regions (Fig. 5, left; Fig. A1). For the 100% vs. 80% predictability difference, significant edges correspond to the right caudal middle frontal gyrus, and right insula regions (Fig. 5, right; Fig. A2).

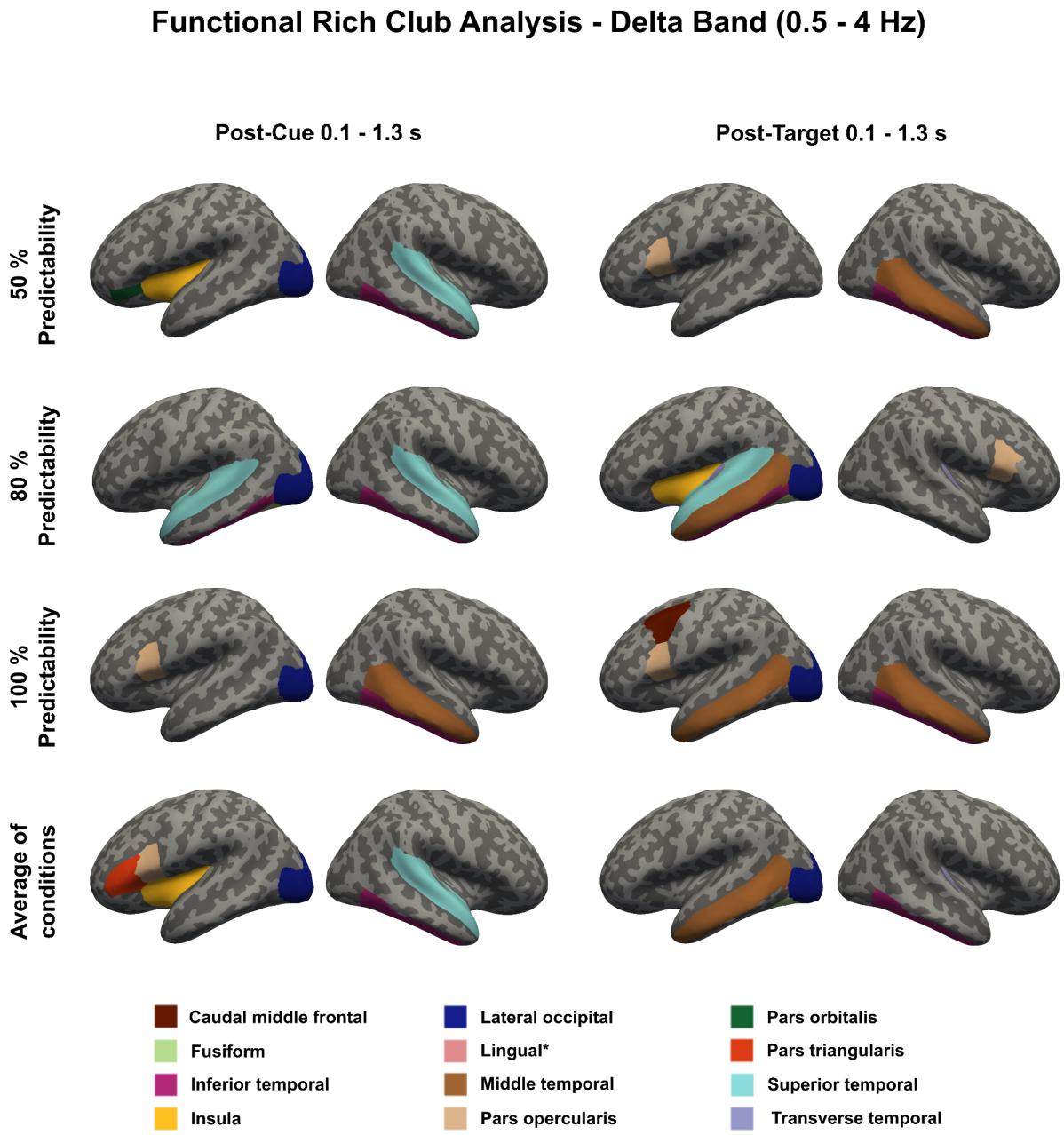

Figure 2. Identified connectivity inflow hub regions for the delta band, post-cue 0.1 - 1.3 s and post-target 0.1 - 1.3 s, based on standardized NDTE values averaged over all epochs of all subjects in a given condition. (The lingual gyrus is not transparent from this view.)

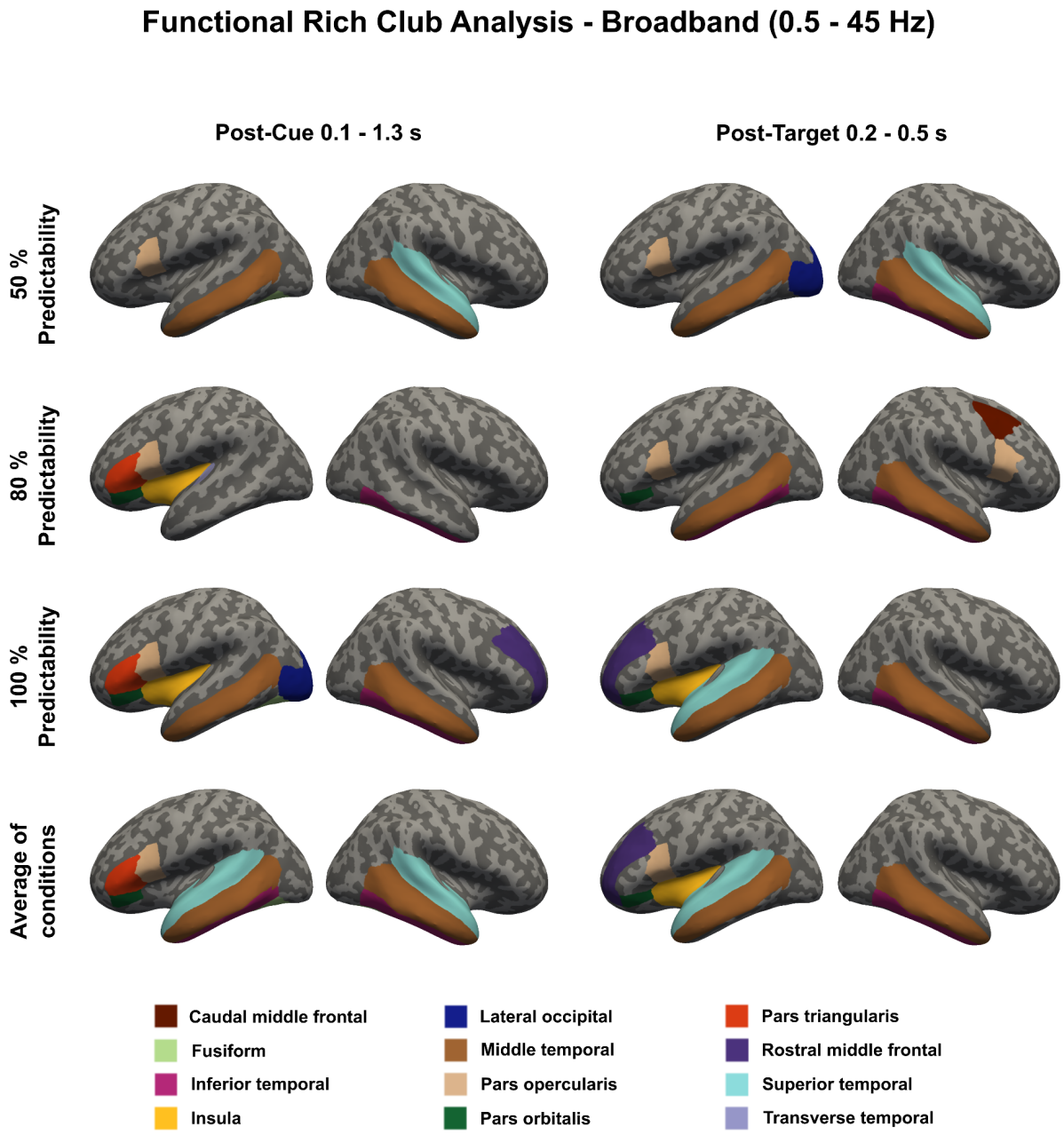

Figure 3. Identified connectivity inflow hub regions for broadband data, post-cue 0.1 - 1.3 s and post-target 0.2 - 0.5 s, based on standardized NDTE values averaged over all epochs of all subjects in a given condition.

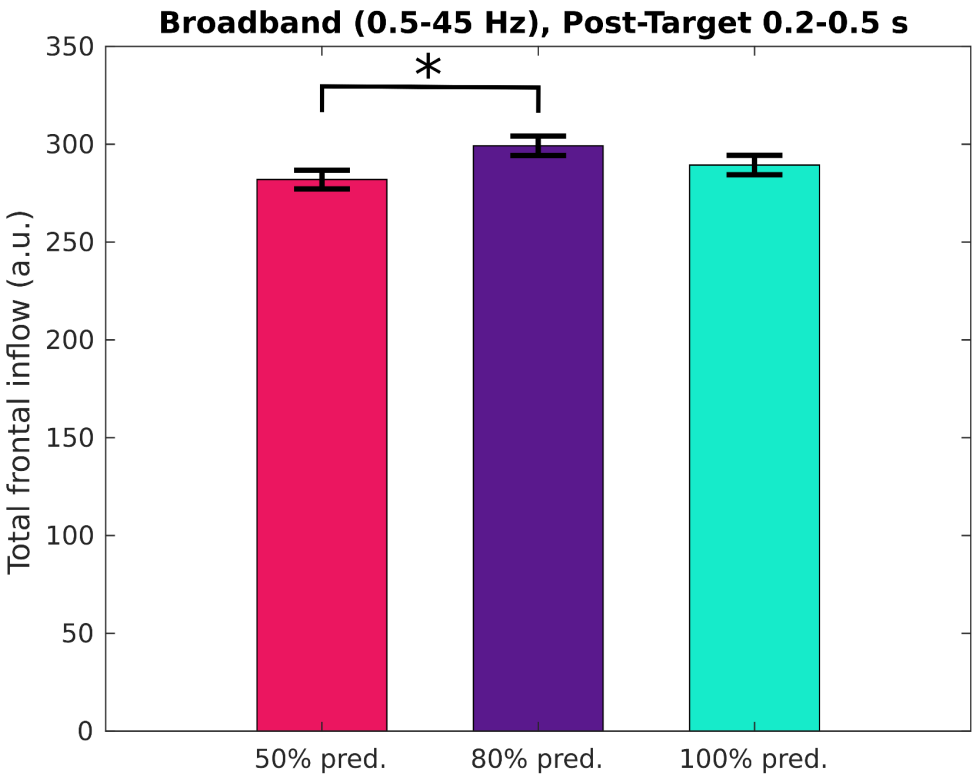

Figure 4. Total information inflow into both hemispheres' frontal regions (caudal middle frontal gyrus, insula, pars opercularis, pars orbitalis, pars triangularis, rostral middle frontal gyrus). The standard error is marked over the average of all subjects and all epochs. The statistically significant difference is marked with an asterisk (*).

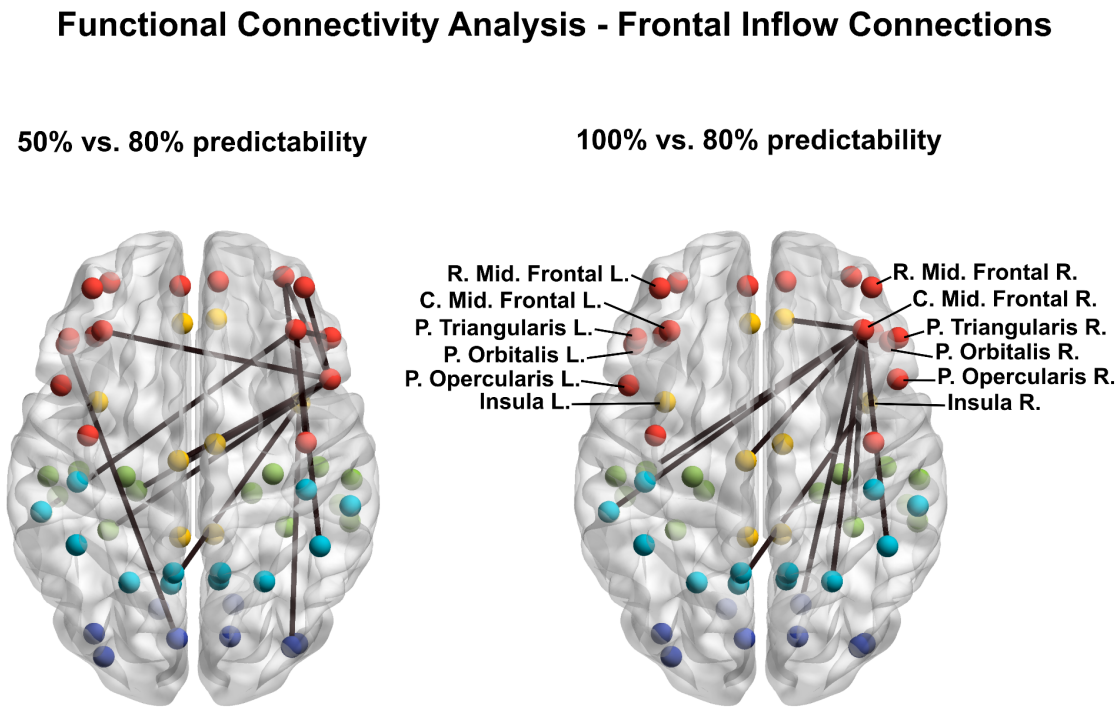

Figure 5. Analysis of frontal inflow connections comparing different conditions for broadband (0.5 - 45 Hz) data in the post-target 0.2 - 0.5 s period. Edges with $p < 0.05$ are shown (corrected against multiple comparisons using the Benjamini-Hochberg method): 50% vs. 80% predictability (left), 100% vs. 80% predictability (right). Spheres on the brain surface show brain regions colored according to cortical lobes: red – frontal, yellow – cingular, light blue – parietal, dark blue – occipital, green – temporal.

4. Discussion

The present study aimed to investigate the role of the frontal and auditory cortices in temporal prediction during auditory perception, using high-density EEG to capture the brain's dynamic responses to varying levels of predictability. By manipulating the timing and predictability of auditory cues and targets, we sought to identify the functional hubs involved in temporal prediction and how these regions influence target detection and anticipation. Our findings demonstrate that the frontal cortex plays a key role in managing temporal predictions, both during the anticipatory phase following a cue and during the actual detection of targets. Importantly, we identified specific frontal regions, such as the MFG (caudal middle frontal gyrus), insula, and IFG (pars opercularis), as major hubs that contribute to integrating sensory input with predictive signals. These results underscore the significance of frontal-sensory interactions in shaping perceptual processes, highlighting how the frontal cortex supports efficient sensory processing through temporal prediction.

4.1. Predictive processing enhances target detection

Our findings demonstrate that temporal prediction significantly improves response speed, aligning with theories of perceptual prediction, which suggest that the brain optimizes processing efficiency when the timing of events is predictable. Our RT results replicate those of Stefanics et al. (2010). Specifically, participants responded faster to early targets when preceded by predictive cues (80% probability) than unpredictive cues (50% probability). This significant difference in RTs indicates that temporal expectancy, driven by the predictive cue, facilitated faster target detection,

underscoring the role of expectation in modulating sensory processing. Moreover, as expected, RTs for late targets were significantly faster than for early targets following unpredictive cues. Late targets were 100% predictable by the time they were presented, allowing participants to fully anticipate their timing, which likely resulted in faster responses. This pattern supports the notion that the high predictability of event timing enables the nervous system to allocate resources more efficiently, leading to improved detection performance (Bar, 2007; Bubic et al., 2010; Schroeder & Lakatos, 2009).

Additionally, the results suggest that participants dynamically updated their temporal expectations. In trials where an early target did not appear, participants shifted their expectation towards the late target, yielding similar RTs for late targets and early targets predicted with high confidence. This finding highlights the brain's ability to adapt to environmental probabilities and optimize sensory processing based on updated temporal information. Overall, these findings provide strong evidence for the impact of predictive processing on target detection, showing that the brain's ability to form temporal predictions enhances sensory efficiency and responsiveness. The significant differences in RTs between conditions of varying predictability emphasize the importance of temporal cues in guiding attention and preparing the sensory system for imminent events (Jones, 2018; Large & Jones, 1999).

4.2. Event-related dynamics during target detection

Our ERP results support the notion that the confidence level at which an event can be predicted affects its processing in the brain. Similarly to the results of Stefanics and colleagues (2010), we found larger P3 responses for targets predicted with lower confidence (Fig. 1C). Beyond the replication of earlier results, our analyses revealed that the cue reliability difference is reflected in separate frontal and parietal electrode clusters, the latter possibly corresponding to P3 responses (Donchin & Coles, 1988; Polich, 2003, 2007; Wronka et al., 2012). The amplitude of the parietal ERP cluster was larger for 50% predictable targets than either 80% or 100% predictable targets. This might suggest that the need for context updating was more pronounced in the less predictable condition (Donchin & Coles, 1988). Alternatively, the clusters can be interpreted as an updating P3 response, reflecting inhibitory mechanisms during attentional selection in preparation for encoding information about the target sounds into memory (Polich, 2007).

Meanwhile, the difference between the two high-predictability conditions was reflected in a lateralized ERP cluster, likely corresponding to motor responses rather than target prediction (VaezMousavi & Barry, 1993). These results align with the RT data in that the processing of targets predicted with 80% and 100% confidence does not seem to evoke different context updating or inhibitory processes, while targets predicted with low confidence evoke different brain responses in both anterior and posterior regions. If an event can be expected with high confidence, processing capacities can be focused on preparing action. In contrast, uncertainty about the time point at which a responsive action is expected prioritizes the enhancement of target identification before motor planning.

4.3. Functional brain networks reflecting the anticipation and detection of auditory events

We demonstrated that the frontal cortex plays a critical role in temporal prediction during both anticipating and detecting auditory events, that is, during the post-cue and post-target phases of a target detection task. The IFG (specifically pars orbitalis) acts as a functional hub duringboth processing phases regardless of the level of predictability. As the predictability of a target auditory event increases, the network widens to include the pars orbitalis and triangularis, as well as the MFG (Fig. 2). While the IFG is involved in detecting and identifying target events (Clarke et al., 1996,

2000; Adriani et al., 2003) and is a key region of the auditory ventral pathway (Arnott et al., 2004; Rauschecker & Tian, 2000), MFG is an important executive center of attentional monitoring (Japee et al, 2015; Song et al., 2019) and movement planning in response to auditory cues (Hosman et al., 2021). Our results demonstrate that the functional connectivity between these areas underlies the predictive processes in anticipating and detecting auditory events. Additionally, frontal regions exhibited distinct connectivity patterns in both post-cue (anticipatory) and post-target (response) phases, indicating that the frontal cortex not only contributes to forming predictions after the cue but also continues to influence processing when the target appears. The present data is in line with integrative approaches of predictive processing in the brain, where both frontal and sensory cortices play a role in temporal predictions (Dürschmid, 2016; Osnes, 2012; Rahnev, 2011).

We found that frontal inflow is a function of target predictability (Fig. 3). Our connectivity analyses revealed differences in information inflow into frontal regions – specifically the caudal MFG, insula, and IFG – based on the predictability manipulation: 80% predictability resulted in different connectivity patterns from both 50% and 100% predictability (Fig. 4). This suggests that these frontal areas are crucial for integrating temporal predictions when these involve a moderate level of uncertainty, while the anticipation and processing of either low-certainty or 100% certain auditory events relies less on frontal inflow, and instead involves network hubs in the temporal cortex (middle [MTG] and superior temporal gyrus [STG]).

Our findings also highlight the frequency specificity of the network hubs observed in the delta and broadband ranges. We observed mainly overlapping hubs across these frequency bands, suggesting that the network structure supporting predictive processing in response to auditory events is shared between delta and broadband frequencies. However, significant differences in functional connectivity emerged only in the broadband analysis, with delta band connectivity failing to show similar significance. This may stem from the very slow oscillations in the delta band, which could be challenging to measure accurately over short EEG epochs. Unlike rapid phase resetting that occurs in response to external events, slow anticipatory processes might rely on functional connections in higher frequency bands, where finer temporal resolution could better capture anticipatory dynamics. Therefore, higher frequencies may contribute critically to anticipatory processes and could complement delta band activity, enabling the nuanced, temporally sensitive coordination of predictive processing (Sauseng & Klimesch, 2008; Arnal et al., 2015; Kaiser et al., 2007).

A more detailed analysis identified specific inflow connections into the frontal cortex that were significantly involved in temporal prediction during the target detection phase at different levels of predictability (Fig. 4). The comparisons and time window of analysis (0.2–0.5 s) followed our ERP analyses, revealing large-scale networks active during the generation of the target detection-related transient responses. In agreement with our ERP results showing a significant involvement of frontal and parietal electrode clusters in target detection (Fig. 1C), our functional connectivity (FC) analyses revealed that frontal hubs primarily receive inflow from posterior regions. Contrasting the detection of 100% and 50% predictable targets, there was a difference in the parietal, cingular and temporal inflow into right caudal MFG, indicating the role of this hub region in integrating auditory associative processing of perception and motor plans (Hosman et al., 2021). The contrast between 50% and 80% predictable targets was reflected in a larger number of frontal inflow hubs, likely reflecting the need for more attentional control and prediction error propagation in the case of a less reliable cue (Ficco et al., 2021).

We also examined the temporal dynamics of the interactions between frontal and sensory regions. The findings suggest that the frontal cortex modulates sensory processing through top-down influences during the anticipation and detection of temporally predictable events, with distinct oscillatory and connectivity patterns reflecting different levels of predictability. Events of uncertain predictability are processed by a similar network in both the anticipation and detection phases,

involving the left IFG and MTG, as well as the right MTG and STG (Fig. 2), reflecting the lack of information in the unreliable cue. In contrast, 80% predictable events involved mainly left frontal areas in the anticipatory phase, while a network of temporal and right frontal regions emerged during target detection. The anticipation of 100% predictable events activated a fronto-temporal network, reflecting intensive top-down information flow in preparation for the target event, with additional left STG involvement during target detection.

In summary, our results support the notion that auditory predictions are processed in a network of frontal and sensory cortical regions (Clark, 2013; Hohwy, 2013). More certain predictions evoke greater frontal contributions during both the anticipation and the detection of auditory events. Frontal areas for auditory object recognition (IFG) and attentional control (MFG) receive an increasing inflow of information as predictability grows. The connectivity of these areas with the temporal cortex reflects the top-down control over auditory perception is a function of cue reliability during predictive coding. Thus the auditory temporal prediction network connects sensory and higher-order brain regions, and its organization is modified by the reliability of the predictions.

Data availability

Preprocessed data, analysis scripts, and results will be publicly available at the OSF repository: https://osf.io/sa7zf/

Declaration of interests

The authors declare no conflicts of interest.

Funding

This work was funded by the Hungarian National Research Development and Innovation Office (ANN131305) to BT; the Office of Naval Research (N62909-23-1-2025) to AB, IW, and PN; and the Austrian Science Fund (FWF, Grant-DOIs 10.55776/I4294 and 10.55776/ZK66) to RB.

Acknowledgments

The authors thank the staff of RCNS (Barbara Matulai and Emese Várkonyi) who recorded the data.

References

Adriani, M. *et al.* (2003) "Sound recognition and localization in man: specialized cortical networks and effects of acute circumscribed lesions," *Experimental Brain Research*, 153(4), pp. 591–604. Available at: https://doi.org/10.1007/s00221-003-1616-0.

Arnal, L.H., Doelling, K.B. and Poeppel, D. (2015) "Delta–Beta Coupled Oscillations Underlie Temporal Prediction Accuracy," *Cerebral Cortex*, 25(9), pp. 3077–3085. Available at: https://doi.org/10.1093/cercor/bhu103.

Arnal, L.H. and Giraud, A.L. (2012) "Cortical oscillations and sensory predictions," *Trends in Cognitive Sciences*, pp. 390–398. Available at: https://doi.org/10.1016/j.tics.2012.05.003.

Arnott, S.R. *et al.* (2004) "Assessing the auditory dual-pathway model in humans," *NeuroImage*, 22(1), pp. 401–408. Available at: https://doi.org/https://doi.org/10.1016/j.neuroimage.2004.01.014.

Bar, M. (2007) "The proactive brain: using analogies and associations to generate predictions," *Trends in cognitive sciences*, 11(7), pp. 280–289.

Benjamini, Y. and Hochberg, Y. (1995) "Controlling the False Discovery Rate: A Practical and Powerful Approach to Multiple Testing," *Journal of the Royal Statistical Society: Series B (Methodological)*, 57(1), pp. 289–300. Available at: https://doi.org/https://doi.org/10.1111/j.2517-6161.1995.tb02031.x.

Brovelli, A. *et al.* (2015) "Characterization of cortical networks and corticocortical functional connectivity mediating arbitrary visuomotor mapping," *Journal of Neuroscience*, 35(37), pp. 12643–12658. Available at: https://doi.org/10.1523/JNEUROSCI.4892-14.2015.

Bubic, A., von Cramon, D.Y. and Schubotz, R.I. (2010) "Prediction, cognition and the brain," *Frontiers in Human Neuroscience*, 4. Available at: https://www.frontiersin.org/journals/human-neuroscience/articles/10.3389/fnhum.2010.00025.

Buzsáki, G. and Draguhn, A. (2004) *Neuronal Oscillations in Cortical Networks*. Available at: https://www.science.org.

Clark, A. (2013) "Whatever next? Predictive brains, situated agents, and the future of cognitive science," *Behavioral and Brain Sciences*, 36(3), pp. 181–204. Available at: https://doi.org/10.1017/S0140525X12000477.

Clarke, S. *et al.* (1996) "Non-verbal auditory recognition in normal subjects and brain-damaged patients: Evidence for parallel processing," *Neuropsychologia*, 34(6), pp. 587–603. Available at: https://doi.org/https://doi.org/10.1016/0028-3932(95)00142-5.

Clarke, S. *et al.* (2000) "Auditory agnosia and auditory spatial deficits following left hemispheric lesions: evidence for distinct processing pathways," *Neuropsychologia*, 38(6), pp. 797-807. Available at: www.elsevier.com/locate/neuropsychologia.

Coull, J.T., Cotti, J. and Vidal, F. (2016) "Differential roles for parietal and frontal cortices in fixed versus evolving temporal expectations: Dissociating prior from posterior temporal probabilities with fMRI," *NeuroImage*, 141, pp. 40–51. Available at: https://doi.org/https://doi.org/10.1016/j.neuroimage.2016.07.036.

Dale, A.M. *et al*. (2000). “Dynamic statistical parametric mapping: combining fMRI and MEG for high-resolution imaging of cortical activity,”. *Neuron,* 26(1), pp. 55-67.

Deco, G. *et al.* (2022) “The INSIDEOUT framework provides precise signatures of the balance of intrinsic and extrinsic dynamics in brain states,” *Communications Biology*, 5(1). Available at: https://doi.org/10.1038/s42003-022-03505-7.

Deco, G., Vidaurre, D. and Kringelbach, M.L. (2021) “Revisiting the global workspace orchestrating the hierarchical organization of the human brain,” *Nature Human Behaviour*, 5(4), pp. 497–511. Available at: https://doi.org/10.1038/s41562-020-01003-6.

Delorme, A., Sejnowski, T. and Makeig, S. (2007) “Enhanced detection of artifacts in EEG data using higher-order statistics and independent component analysis,” *NeuroImage*, 34(4), pp. 1443–1449. Available at: https://doi.org/10.1016/j.neuroimage.2006.11.004.

Donchin, E. and Coles, M.G.H. (1988) “Is the P300 component a manifestation of context updating?,” *Behavioral and Brain Sciences*. 2010/02/04 edn, 11(3), pp. 357–374. Available at: https://doi.org/10.1017/S0140525X00058027.

Dürschmid, S. *et al.* (2016) “Hierarchy of prediction errors for auditory events in human temporal and frontal cortex,” *Proceedings of the National Academy of Sciences*, 113(24), pp. 6755–6760. Available at: https://doi.org/10.1073/pnas.1525030113.

Ficco, L. *et al.* (2021) “Disentangling predictive processing in the brain: a meta-analytic study in favour of a predictive network,” *Scientific Reports*, 11(1), p. 16258. Available at: https://doi.org/10.1038/s41598-021-95603-5.

Fischl, B. (2012) “FreeSurfer,” *NeuroImage*, 62(2), pp. 774–781. Available at: https://doi.org/https://doi.org/10.1016/j.neuroimage.2012.01.021.

Fuchs, M. *et al.* (1998) “An improved boundary element method for realistic volume-conductor modeling,” *IEEE Transactions on Biomedical Engineering*, 45(8), pp. 980–997. Available at: https://doi.org/10.1109/10.704867.

Fuchs, M. *et al.* (2002) “A standardized boundary element method volume conductor model,” *Clinical neurophysiology,* 113(5), pp. 702-712.”Available at: www.mni.mcgill.ca.

Gramfort, A. *et al.* (2010) “OpenMEEG: opensource software for quasistatic bioelectromagnetics,” *BioMedical Engineering OnLine*, 9(1), p. 45. Available at: https://doi.org/10.1186/1475-925X-9-45.

van den Heuvel, M.P. and Sporns, O. (2011) “Rich-club organization of the human connectome,” *Journal of Neuroscience*, 31(44), pp. 15775–15786. Available at: https://doi.org/10.1523/JNEUROSCI.3539-11.2011.

Hohwy, J. (2013) *The predictive mind*. OUP Oxford.

Hosman, T. *et al.* (2021) “Auditory cues reveal intended movement information in middle frontal gyrus neuronal ensemble activity of a person with tetraplegia,” *Scientific Reports*, 11(1). Available at: https://doi.org/10.1038/s41598-020-77616-8.

Huang, Y., Parra, L.C. and Haufe, S. (2016) "The New York Head—A precise standardized volume conductor model for EEG source localization and tES targeting," *NeuroImage*, 140, pp. 150–162. Available at: https://doi.org/https://doi.org/10.1016/j.neuroimage.2015.12.019.

Ignatiadis, K. *et al.* (2024) "Threat-Related Corticocortical Connectivity Elicited by Rapid Auditory Looms," *bioRxiv*, 2024–06.

Japee, S. *et al.* (2015) "A role of right middle frontal gyrus in reorienting of attention: A case study," *Frontiers in Systems Neuroscience*, 9(MAR). Available at: https://doi.org/10.3389/fnsys.2015.00023.

Jones, M.R. (2018) *Time will tell: A theory of dynamic attending*. Oxford University Press.

Kaiser, J. *et al.* (2007) "Prefrontal gamma-band activity distinguishes between sound durations," *Brain Research*, 1139, pp. 153–162. Available at: https://doi.org/https://doi.org/10.1016/j.brainres.2006.12.085.

Klein, A. and Tourville, J. (2012) "101 labeled brain images and a consistent human cortical labeling protocol," *Frontiers in Neuroscience* 6, 171. Available at: https://doi.org/10.3389/fnins.2012.00171.

Kok, P., Jehee, J.F.M. and de Lange, F.P. (2012) "Less Is More: Expectation Sharpens Representations in the Primary Visual Cortex," *Neuron*, 75(2), pp. 265–270. Available at: https://doi.org/10.1016/j.neuron.2012.04.034.

Kononowicz, T.W. and Penney, T.B. (2016) "The contingent negative variation (CNV): timing isn't everything," *Current Opinion in Behavioral Sciences*, 8, pp. 231–237. Available at: https://doi.org/https://doi.org/10.1016/j.cobeha.2016.02.022.

Lakatos, P. *et al.* (2005) "An Oscillatory Hierarchy Controlling Neuronal Excitability and Stimulus Processing in the Auditory Cortex," *Journal of Neurophysiology*, 94(3), pp. 1904–1911. Available at: https://doi.org/10.1152/jn.00263.2005.

de Lange, F.P., Heilbron, M. and Kok, P. (2018) "How Do Expectations Shape Perception?," *Trends in Cognitive Sciences*, 22(9), pp. 764–779. Available at: https://doi.org/10.1016/j.tics.2018.06.002.

Large, E.W. and Jones, M.R. (1999) "The dynamics of attending: How people track time-varying events.," *Psychological review*, 106(1), p. 119.

Mantini, D. *et al.* (2010) "Multimodal integration of fMRI and EEG data for high spatial and temporal resolution analysis of brain networks," *Brain Topography*, 23(2), pp. 150–158. Available at: https://doi.org/10.1007/s10548-009-0132-3.

Maris, E. and Oostenveld, R. (2007) "Nonparametric statistical testing of EEG- and MEG-data," *Journal of Neuroscience Methods*, 164(1), pp. 177–190. Available at: https://doi.org/https://doi.org/10.1016/j.jneumeth.2007.03.024.

Meirhaeghe, N., Sohn, H. and Jazayeri, M. (2021) "A precise and adaptive neural mechanism for predictive temporal processing in the frontal cortex," *Neuron*, 109(18), pp. 2995-3011.e5. Available at: https://doi.org/10.1016/j.neuron.2021.08.025.

Murray, P.D. and Keller, A. (2011) "Somatosensory response properties of excitatory and inhibitory neurons in rat motor cortex," *J Neurophysiol*, 106, pp. 1355–1362. Available at: https://doi.org/10.1152/jn.01089.2010.

Osnes, B. *et al.* (2012) "Stimulus expectancy modulates inferior frontal gyrus and premotor cortex activity in auditory perception," *Brain and Language*, 121(1), pp. 65–69. Available at: https://doi.org/https://doi.org/10.1016/j.bandl.2012.02.002.

Philiastides, M.G. and Sajda, P. (2007) "EEG-informed fMRI reveals spatiotemporal characteristics of perceptual decision making," *Journal of Neuroscience*, 27(48), pp. 13082–13091. Available at: https://doi.org/10.1523/JNEUROSCI.3540-07.2007.

Pizzagalli, D.A. (2007) "Electroencephalography and high-density electrophysiological source localization.," in *Handbook of psychophysiology, 3rd ed.* New York, NY, US: Cambridge University Press, pp. 56–84. Available at: https://doi.org/10.1017/CBO9780511546396.003.

Polich, J. (2003) "Theoretical overview of P3a and P3b," *Detection of change: Event-related potential and fMRI findings*, pp. 83–98.

Polich, J. (2007) "Updating P300: an integrative theory of P3a and P3b," *Clinical neurophysiology*, 118(10), pp. 2128–2148.

Quiroga, R.Q., Kreuz, T. and Grassberger, P. (2002) "Event synchronization: a simple and fast method to measure synchronicity and time delay patterns," *Physical review E*, 66(4), p. 041904.

Rahnev, D., Lau, H. and de Lange, F.P. (2011) "Prior Expectation Modulates the Interaction between Sensory and Prefrontal Regions in the Human Brain," *The Journal of Neuroscience*, 31(29), p. 10741. Available at: https://doi.org/10.1523/JNEUROSCI.1478-11.2011.

Rao, R.P., and Ballard, D.H. (1999) "Predictive coding in the visual cortex: a functional interpretation of some extra-classical receptive-field effects," *Nature neuroscience*, 2(1), 79-87.

Rauschecker, J.P. and Tian, B. (2000) "Mechanisms and streams for processing of 'what' and 'where' in auditory cortex," *Proceedings of the National Academy of Sciences*, 97(22), pp. 11800–11806. Available at: https://doi.org/10.1073/pnas.97.22.11800.

Sauseng, P. and Klimesch, W. (2008) "What does phase information of oscillatory brain activity tell us about cognitive processes?," *Neuroscience & Biobehavioral Reviews*, 32(5), pp. 1001–1013. Available at: https://doi.org/https://doi.org/10.1016/j.neubiorev.2008.03.014.

Schroeder, C.E. and Lakatos, P. (2009) "The gamma oscillation: Master or slave?," *Brain Topography*, 22(1), pp. 24–26. Available at: https://doi.org/10.1007/s10548-009-0080-y.

Song, J. *et al.* (2015) "EEG source localization: Sensor density and head surface coverage," *Journal of Neuroscience Methods*, 256, pp. 9–21. Available at: https://doi.org/10.1016/j.jneumeth.2015.08.015.

Song, P. *et al.* (2019) "Transcranial magnetic stimulation to the middle frontal gyrus during attention modes induced dynamic module reconfiguration in brain networks," *Frontiers in Neuroinformatics*, 13. Available at: https://doi.org/10.3389/fninf.2019.00022.

Stefanics, G. *et al.* (2010) "Phase entrainment of human delta oscillations can mediate the effects of expectation on reaction speed," *Journal of Neuroscience*, 30(41), pp. 13578–13585. Available at: https://doi.org/10.1523/JNEUROSCI.0703-10.2010.

Tadel, F. *et al.* (2011) "Brainstorm: A User-Friendly Application for MEG/EEG Analysis," *Computational Intelligence and Neuroscience*, 2011, pp. 1–13. Available at: https://doi.org/10.1155/2011/879716.

Toosi, T., Tousi, E.K. and Esteky, H. (2017) "Learning temporal context shapes prestimulus alpha oscillations and improves visual discrimination performance," *J Neurophysiol*, 118, pp. 771–777. Available at: https://doi.org/10.1152/jn.00969.2016.

Tóth, B. *et al.* (2020) "The effects of speech processing units on auditory stream segregation and selective attention in a multi-talker (cocktail party) situation," *Cortex*, 130, pp. 387–400.

Tukey, J.W. (1949) "Comparing Individual Means in the Analysis of Variance," *Biometrics*, 99-114. Available at: https://www.jstor.org/stable/3001913.

VaezMousavi, S.M. and Barry, R.J. (1993) "Positive and negative shifts of the readiness potential: preparatory effects," *International journal of psychophysiology*, 15(2), pp. 105–113.

Walter, W.G. *et al.* (1964) "Contingent negative variation: an electric sign of sensori-motor association and expectancy in the human brain," *nature*, 203(4943), pp. 380–384.

Wiener, M. and Kanai, R. (2016) "Frequency tuning for temporal perception and prediction," *Current Opinion in Behavioral Sciences*, 8, pp. 1–6. Available at: https://doi.org/https://doi.org/10.1016/j.cobeha.2016.01.001.

Wronka, E.A., Kaiser, J. and Coenen, A.M.L. (2012) "Neural generators of the auditory evoked potential components P3a and P3b."

Supplementary material

Table A1: Identified connectivity inflow hub regions for the delta band (0.5 - 4 Hz) in the post-cue 0.1-1.3 s period.

Condition	Hub regions
50% Predictability	Insula L Lateraloccipital L Inferiortemporal R Parsorbitalis L Superiortemporal R
80% Predictability	Inferiortemporal L Lingual L Fusiform L Lateraloccipital L Superiortemporal L Inferiortemporal R Superiortemporal R

100% Predictability	Parsopercularis L Inferiortemporal R Lateraloccipital L Fusiform R Middletemporal R
Average of all conditions	Lateraloccipital L Inferiortemporal R Parsopercularis L Insula L Parstriangularis L Superiortemporal R

Table A2: Identified connectivity inflow hub regions for the delta band (0.5 - 4 Hz) in the post-target 0.1-1.3 s period.

Condition	Hub regions
50% Predictability	Parsopercularis L Middletemporal R Inferiortemporal R
80% Predictability	Middletemporal L Transversetemporal L Fusiform L Superiortemporal L Inferiortemporal L Lateraloccipital L Insula L Transversetemporal R Parsopercularis R Lingual L
100% Predictability	Lateraloccipital L Inferiortemporal R Lingual L Middletemporal L Caudalmiddlefrontal L Parsopercularis L Middletemporal R
Average of all conditions	Lateraloccipital L Middletemporal L Fusiform L Inferiortemporal R Transversetemporal R

Table A3: Identified connectivity inflow hub regions for broadband (0.5 - 45 Hz) data in the post-cue 0.1-1.3 s period.

Condition	Hub regions
50% Predictability	Parsopercularis L

	Lingual L Middletemporal R Fusiform L Superiortemporal R Middletemporal L
80% Predictability	Parsopercularis L Parsorbitalis L Insula L Fusiform R Inferiortemporal R Parstriangularis L Transversetemporal L
100% Predictability	Parsopercularis L Inferiortemporal R Middletemporal R Rostralmiddlefrontal R Fusiform L Middletemporal L Insula L Parsorbitalis L Lateraloccipital L Parstriangularis L
Average of all conditions	Parsopercularis L Inferiortemporal R Middletemporal R Parsorbitalis L Fusiform L Middletemporal L Fusiform R Inferiortemporal L Parstriangularis L Superiortemporal L Superiortemporal R

Table A4: Identified connectivity inflow hub regions for broadband (0.5 - 45 Hz) data in the post-target 0.2 - 0.5 s period.

Condition	Hub regions
50% Predictability	Parsopercularis L Middletemporal R Lateraloccipital L Middletemporal L Superiortemporal R Inferiortemporal R
80% Predictability	Middletemporal L Parsopercularis R Inferiortemporal R Parsorbitalis L

	Caudalmiddlefrontal R Middletemporal R Inferiortemporal L Parsopercularis L
100% Predictability	Inferiortemporal R Parsopercularis L Parsorbitalis L Rostralmiddlefrontal L Middletemporal L Insula L Middletemporal R Superiortemporal L
Average of all conditions	Middletemporal L Parsopercularis L Inferiortemporal R Middletemporal R Insula L Rostralmiddlefrontal L Parsorbitalis L Superiortemporal L

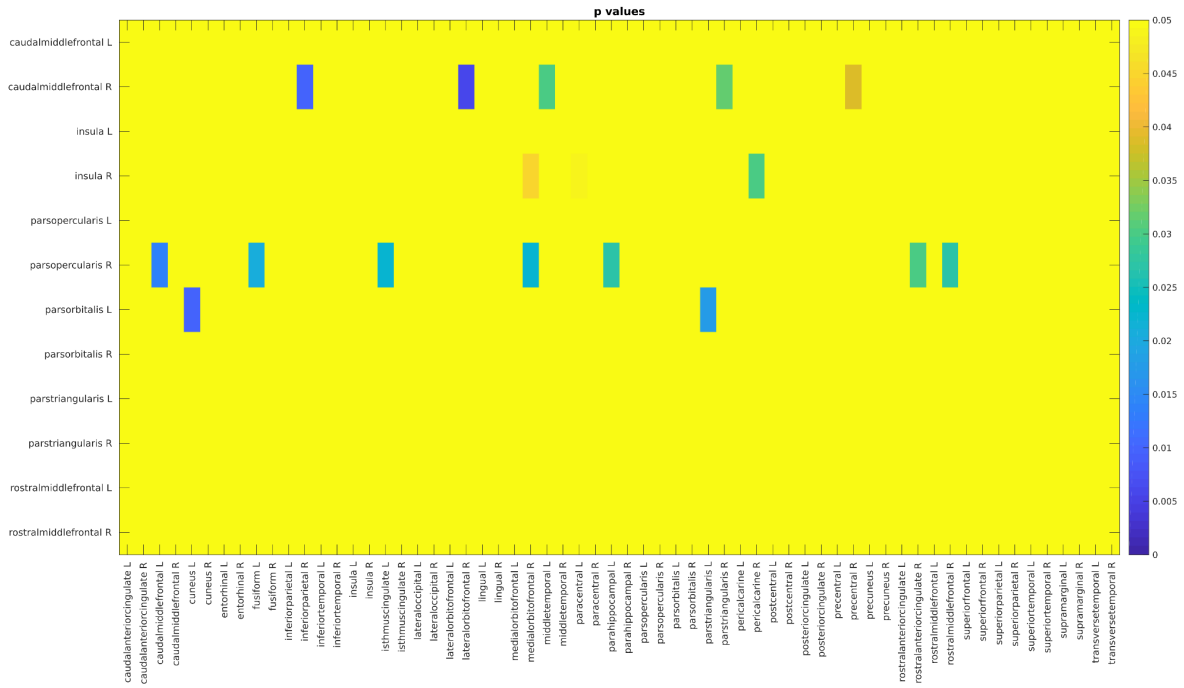

Figure A1. Analysis of frontal inflow connections comparing the 50% vs. 80% predictability conditions for broadband (0.5 - 45 Hz) data in the post-target 0.2 - 0.5 s period. Edges with $p < 0.05$ are shown (corrected against multiple comparisons using the Benjamini-Hochberg method).

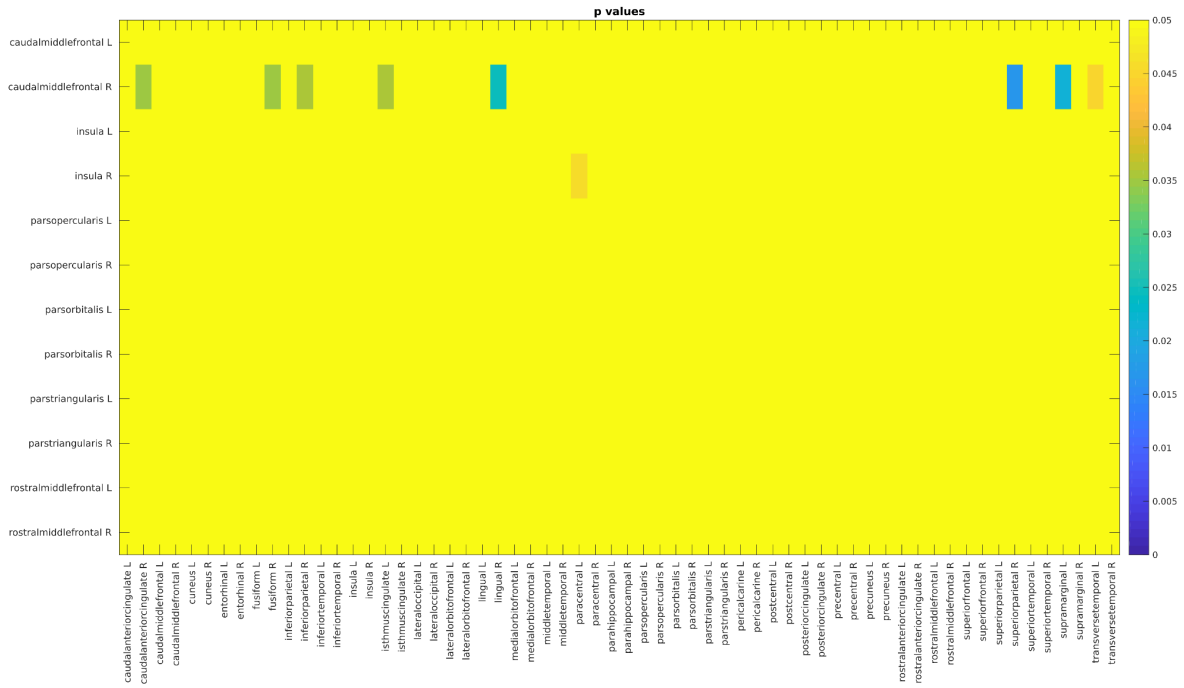

Figure A2. Analysis of frontal inflow connections comparing the 80% vs. 100% predictability conditions for broadband (0.5 - 45 Hz) data in the post-target 0.2 - 0.5 s period. Edges with $p < 0.05$ are shown (corrected against multiple comparisons using the Benjamini-Hochberg method).